Supporting Information

Unveiling the time scale of the R-T transition in human hemoglobin

M. Cammarata[a,b,1], M. Levantino[c], M. Wulff[a], A. Cupane[c,*]

[a]*European Synchrotron Radiation Facility, Grenoble, France*
[b]*Centre for Molecular Movies, University of Copenhagen, Denmark*
[c]*Dept. of Physical and Astronom. Sci., University of Palermo, Via Archirafi 36, I-90123 Palermo, Italy*

S1. Experimental Setup

S1.1. X-ray source and mechanical isolation of X-ray pulses

The European Synchrotron Radiation Facility (ESRF) operates its electron storage ring at 6 GeV. With this electron energy, a U17 in-vacuum undulator (17 mm period; SmCo magnets) set to 9 mm gap produces an X-ray spectrum that is sharply peaked at 18.25 keV, but has a long wavelength tail (Figure S1). The spectrum is quasi-monoenergetic with a relative bandwidth of 3.5%. In order to reduce the acquisition time, we took advantage of the full X-ray spectrum which is 250 times more intense compared to a standard monochromatic beam. Note that the loss of information in relaxing the bandwidth to 3.5% is minor due to the orientational disorder of molecules in solution [1]. A Pt-coated toroidal mirror, set at the incidence angle 2.668 mrad, focuses the radiation onto the sample. To minimize distortion of the toroidal mirror from the heat load from the undulator ($\sim$100 W) and ti void overheating of the fast (un-cooled) high speed rotor, a synchronous heat-load chopper was positioned upstream of the mirror; it reduces the average heat load on the mirror and high-speed chopper (see below) by a factor 20 without affecting the pulses used in the pump probe experiment. When operated in 16-bunch mode, the ID09B beamline optics focuses 10^9 X-ray photons in a single pulse down to an elliptical spot as small as 0.06x0.1 mm^2 (vertical x horizontal, FWHM) at the sample position. Quasi-monochromatic X-ray pulses (100 ps long) can be extracted from the high frequency pulse train when the storage ring is filled with either 4 or 16 electron bunches by using a high speed synchronized rotor (high-speed chopper) [2] spinning at $\sim$1 kHz (360th sub-harmonic of the time needed for a single electron bunch to complete the storage ring orbit). To be able to measure time-delays longer than 1 ms, and to allow our sample positioning system to move the sample into a fresh position at every shot, the repetition rate is further reduced by using a "millisecond" shutter. This lowers the repetition rate from 1 kHz down to 0-20 Hz.

S1.2. Laser photolysis

The protein sample was photolyzed with a circularly-polarized (via $\lambda/4$ waveplate), 527 nm laser pulse (DM-50, Laser Photonics). At this excitation wavelength, the decadic extinction coefficient for HbCO and deoxyHb are respectively: $\varepsilon_{CO} = 2.77$ and $\varepsilon_{deoxy} = 1.87$ ($mM^{-1} cm^{-1}$, Hb concentration in tetramers). The temporal and spatial profile of the photolysis laser are shown in Figure S2. Samples were loaded into X-ray capillaries (wall thickness = 10 μm) as shown in Figure S3. Two CO-bubbles of about 1 cm each surrounded the sample to ensure full saturation of the solution. A "protective plug" of CO-saturated glycerol was used to slow down diffusion of gases that might leak through the capillary sealing wax. To maximize the overlap between the pump- and probe-illuminated volumes, orthogonal pump-probe geometry was employed. The X-ray beam penetrated the 2 mm diameter capillary 0.2 mm below its top edge, its path length through the capillary was 1.2 mm. The energy of the laser pulse for the different experiments is reported in Table S1. The sample was maintained at 22 °C. To dilute any X-ray radiation damage over a large sample volume, the sample was translated back and forth along its long axis over a 25 mm

---

*corresponding author
Email address:* cupane@fisica.unipa.it (A. Cupane)
[1]Current address: SLAC National Accelerator Laboratory, Menlo Park, CA, USA

buffer concentration (M)	0.1	0.1	0.1	0.1	0.1
kind of buffer	HEPES	HEPES	K-pho	K-pho	K-pho
Hb concentration (mM of tetramers)	0.57	0.70	0.25	0.50	1.00
pH of the solution	8.5	7.0	7.0	7.0	7.0
Laser energy (mJ)	1.0	1.2	0.54	1.0	2.1

Table S1: Parameters of the data collection.

1 range. To ensure that successive pulses in the 5-10 Hz pulse train excite adjacent but spatially-
2 separated sample volumes in the capillary, the latter was translated by 0.35 mm after each probe
3 pulse. While translating, the cylindrical quartz capillary containing the sample undergoes small
4 (micrometric) vibrations (perpendicularly with respect to the incoming X-rays direction). The
5 scattering signal is affected by these vibrations since the pathlength of X-rays through the sample
6 changes if the capillary gets lower or higher. In order to test this hypothesis, we have measured
7 the static scattering pattern of a sample as a function of the capillary position with respect to the
8 X-ray beam without translating the capillary. The difference between two such scattering patterns
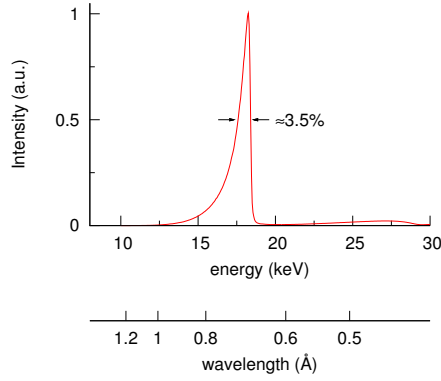9 resembles the fourth SVD component.

Figure S1: Spectrum of the X-ray beam produced by the U17 undulator operated with a 9 mm gap.

10 **S2. Data collected under different experimental conditions and relative analysis**

11 Typical difference signals (laser on - laser off) obtained at selected time delays after photolysis for
12 the various samples investigated are reported in Figure S4. Fits obtained by using the two-state
13 kinetic model described in the main text and in Section S3 of this document are shown in Figures
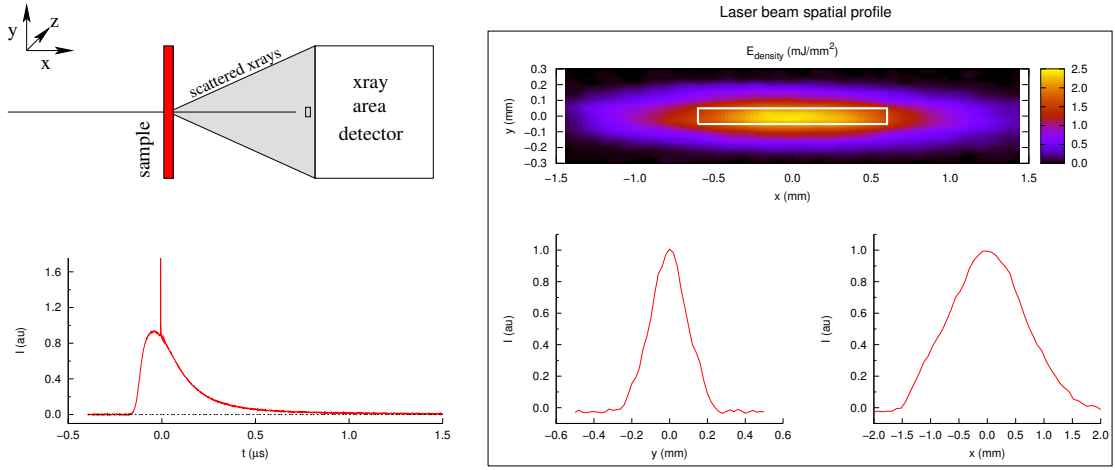14 S5-S8.

Figure S2: Left panel: temporal profile of the laser pulse used to photolyze the sample. The trace has been recorded with a nominal laser–to–Xray pulse time delay of zero; the spike represents the X-ray pulse (100 ps long). Right panel: spatial profile of the laser beam; right scale: energy density (mJ/mm^2) at the sample surface; the white rectangle represents the X-ray probed region. Lower panels: normalized cuts along the x and y directions.
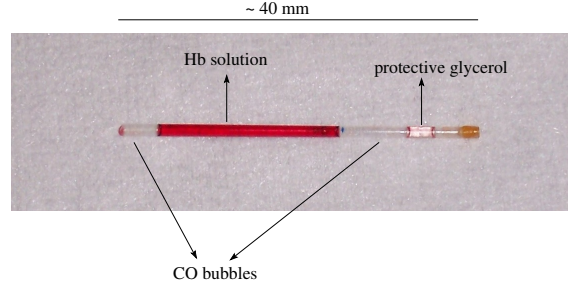

Figure S3: Example of HbCO sample loaded into the capillary

S3. Two-state kinetic model and numerical routines

This kinetic model is adapted from [3]. It is described by the following equations:

$$
\begin{cases}
\partial[CO]/\partial t &= -\sum_{k=0}^{3} -k\,D_R[CO][R_i] \quad -\sum_{k=0}^{3} -k\,D_T[CO][T_i] \\[2mm]
\partial[R_0]/\partial t &= -K_{R_0 \to T_0}[R_0] & -4\,D_R[CO][R_0] & +\left(K_{R_0 \to T_0}/L\right)[T_0] \\[2mm]
\partial[R_1]/\partial t &= -\left(K_{R_0 \to T_0}/s^1\right)[R_1] & +4\,D_R[CO][R_0] & -3\,D_R[CO][R_1] & +\left(K_{R_0 \to T_0}/L\right)\cdot\left(1/(s\,c)^1\right)[T_1] \\[2mm]
\partial[R_2]/\partial t &= -\left(K_{R_0 \to T_0}/s^2\right)[R_2] & +3\,D_R[CO][R_1] & -2\,D_R[CO][R_2] & +\left(K_{R_0 \to T_0}/L\right)\cdot\left(1/(s\,c)^2\right)[T_2] \\[2mm]
\partial[R_3]/\partial t &= -\left(K_{R_0 \to T_0}/s^3\right)[R_3] & +2\,D_R[CO][R_2] & -1\,D_R[CO][R_3] & +\left(K_{R_0 \to T_0}/L\right)\cdot\left(1/(s\,c)^3\right)[T_3] \\[2mm]
\partial[R_4]/\partial t &= -\left(K_{R_0 \to T_0}/s^4\right)[R_4] & +1\,D_R[CO][R_3] & & +\left(K_{R_0 \to T_0}/L\right)\cdot\left(1/(s\,c)^4\right)[T_4] \\[2mm]
\partial[T_0]/\partial t &= +K_{R_0 \to T_0}[R_0] & & -4\,D_T[CO][T_0] & -\left(K_{R_0 \to T_0}/L\right)[T_0] \\[2mm]
\partial[T_1]/\partial t &= +\left(K_{R_0 \to T_0}/s^1\right)[R_1] & +4\,D_T[CO][T_0] & -3\,D_T[CO][T_1] & -\left(K_{R_0 \to T_0}/L\right)\cdot\left(1/(s\,c)^1\right)[T_1] \\[2mm]
\partial[T_2]/\partial t &= +\left(K_{R_0 \to T_0}/s^2\right)[R_2] & +3\,D_T[CO][T_1] & -2\,D_T[CO][T_2] & -\left(K_{R_0 \to T_0}/L\right)\cdot\left(1/(s\,c)^2\right)[T_2] \\[2mm]
\partial[T_3]/\partial t &= +\left(K_{R_0 \to T_0}/s^3\right)[R_3] & +2\,D_T[CO][T_2] & -1\,D_T[CO][T_3] & -\left(K_{R_0 \to T_0}/L\right)\cdot\left(1/(s\,c)^3\right)[T_3] \\[2mm]
\partial[T_4]/\partial t &= +\left(K_{R_0 \to T_0}/s^4\right)[R_4] & +1\,D_T[CO][T_3] & & -\left(K_{R_0 \to T_0}/L\right)\cdot\left(1/(s\,c)^4\right)[T_4]
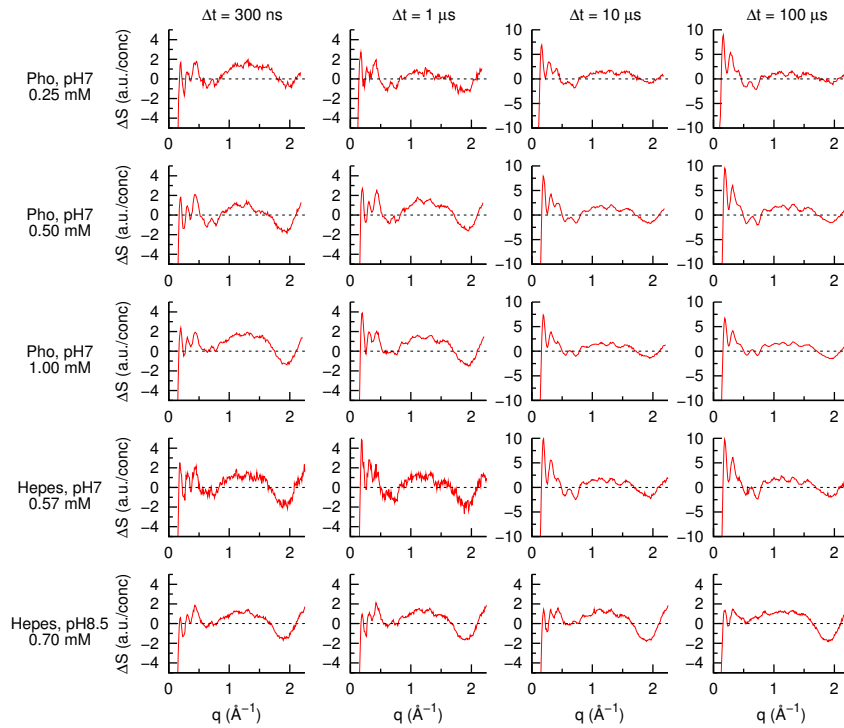\end{cases}
\tag{1}
$$

Figure S4: Example of data measured at selected time delays for the different samples.
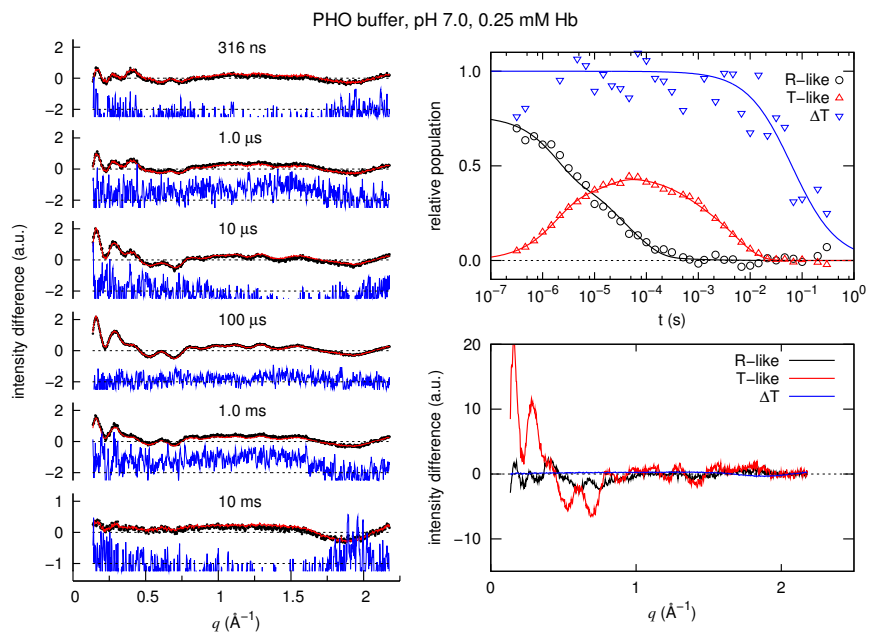

Figure S5: Left panel: fits of data relative to the 0.25 mM Hb sample in 0.1 M phosphate buffer at pH 7. Right panels: (top) time dependence of R-like, T-like, and ΔT (see main text) as calculated from the best fit parameters; (bottom) corresponding basis spectra.
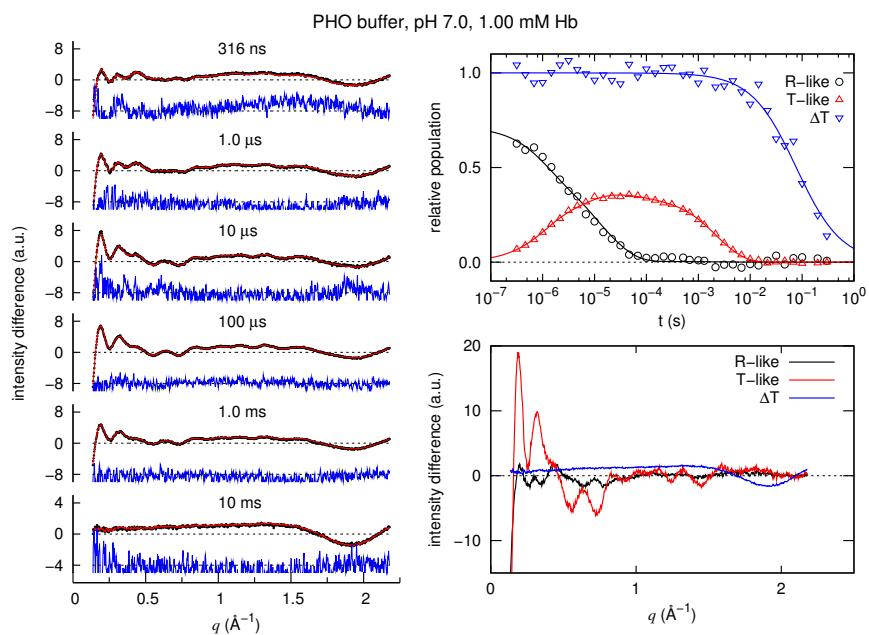
Figure S6: Fittings of data relative to the 1.00 mM Hb sample in 0.1 M phosphate buffer at pH 7; panels as in Figure S5.
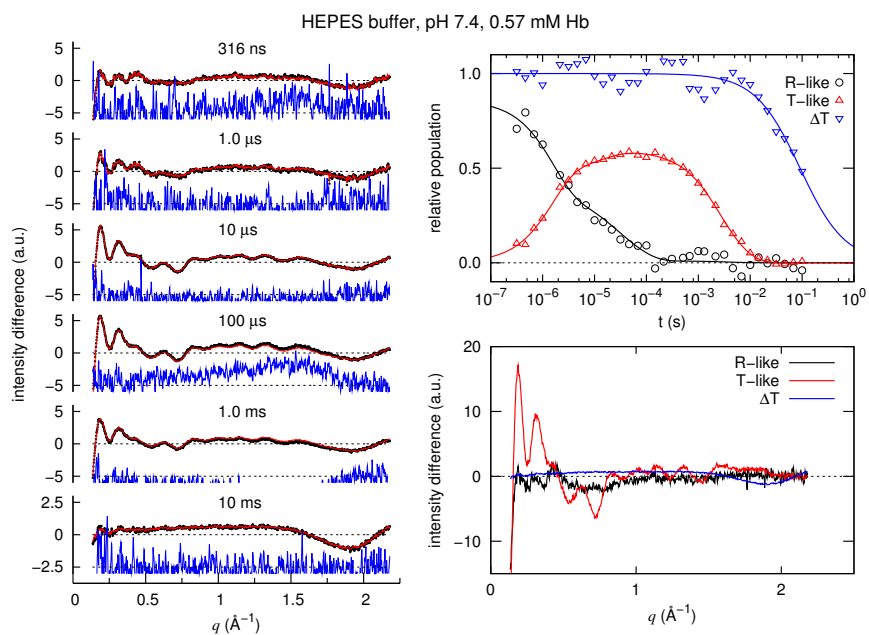

Figure S7: Fittings of data relative to the 0.57 mM Hb sample in 0.1 M HEPES buffer at pH 7.4; panels as in Figure S5.
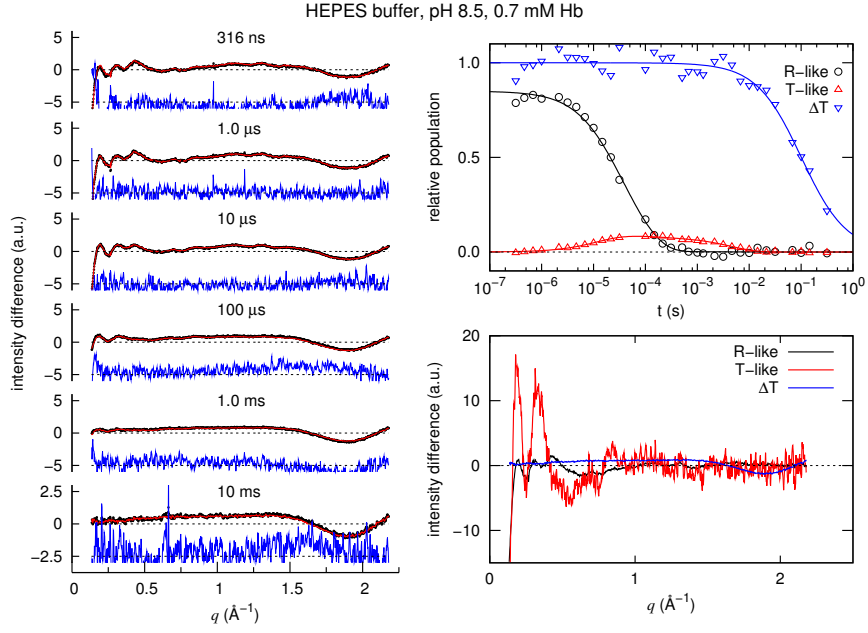
Figure S8: Fittings of data relative to the 0.7 mM Hb sample in 0.1 M HEPES buffer at pH 8.5; panels as in Figure S5.

1   The above system has been solved numerically with the following initial parameters:

$$\begin{cases} [R_i](t=0) & = & \frac{n! \cdot i!}{(n-i)!} N_0^i \cdot (1-N_0)^{n-i} \\ [T_i](t=0) & = & 0 \end{cases} \tag{2}$$

where N_0 is the fraction of deoxyhemes after the pump pulse, using the explicit Jacobian and a requested absolute precision of 10^{-15}. The time dependence of the temperature jump has been assumed to be [4]:

$$Temp(t) = \frac{1}{1 + t/\tau_T} \tag{3}$$

2   The fitting program has been implemented in C++ and used the following libraries:

3   • LSODE as provided by Octave 3.0 (to solve the system of differential equations) [5]

4   • Newmat 11 (for matrix calculation/inversion) [6]

5   • Minuit 1.7.9 (for χ^2 minimization) [7]

6 A block diagram of the fitting approach is shown in Figure S9.

7   The fitting program calculates all $R_i(t)$ and $T_i(t)$ and the concentration of CO in solution.
8 These quantities are used to calculate the $R_{like}(t)$ and $T_{like}(t)$ as discussed in the main text. As
9 an example, Figure S10 shows $R_i(t)$, $T_i(t)$, and $[CO](t)$ obtained by fitting the data relative to the
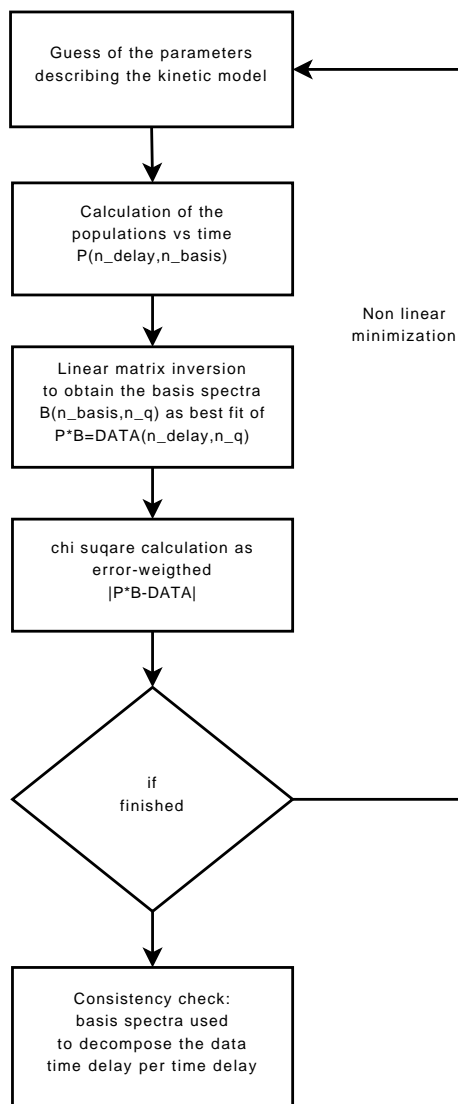10 0.5 mM Hb sample in 0.1 M phosphate buffer at pH 7.

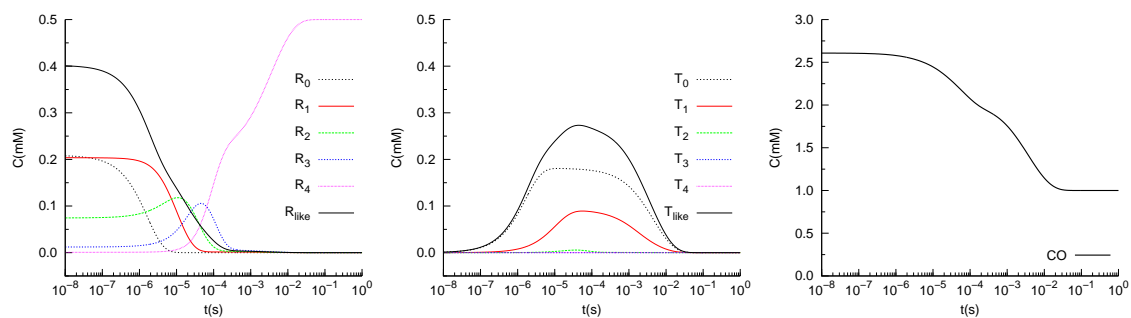Figure S9: Scheme of the fitting procedure

Figure S10: Time dependence for the different states as obtained by fitting the data relative to the 0.5 mM Hb sample in 0.1 M phosphate buffer at pH 7.

S4. Three state kinetic model

In the simple two state kinetic model discussed in the main text and in the preceding section, the change in microscopic CO bimolecular rebinding rate from "fast" to "slow" was assumed to occur simultaneously with the main structural change (dimers rotation) from R to T, i.e. at ~ 2 μs. Such assumption can be questioned since many time-resolved optical studies suggest that the change in CO bimolecular rebinding rate occurs at ~ 20 μs, i.e. a factor 10 slower. Moreover, it is important to check how a different model may influence the time scale of the structural transition obtained from the data analysis. To answer these questions, we developed a three-state kinetic model as shown in Figure S11. The basic idea is the following: a new set of species T_R has been added, whose quaternary structure is "T-like" (i.e. structurally indistinguishable, within the current S/N ratio of TR-WAXS data, from the canonical "T") but whose CO bimolecular rebinding rate is still "R-like", i.e. fast. The WAXS-silent transition from fast to slow rebinding species is assumed to occur with a rate $K2$; suitable scaling and allosteric parameters are introduced as shown in Figure S11. These "three-state" kinetic model can be easily implemented in the fitting routine; in analogy with the two-state kinetic model, the following relations have been used: $c_T(t) = \sum_{i=0,4} T_i(t) + \sum_{i=0,4} T_{R_i}(t)$ and $c_{R^*}(t) = \sum_{i=0,4}(4-i)/4\, R_i(t)$. The three-state kinetic model is able to give good fitting of the data with reasonable parameters value (Table S2). In particular, the fitting shown in Figure S12 has a 20 μs time scale for the T_{R_0} to T_0 transition, while the time scale for the main structural transition, R_0 to T_{R_0}, remains 2.1 μs (see Table S2). Use of different time scales for the T_{R_0} to T_0 transition gives fits of comparable quality; however, in all these fittings, the time scale of the main structural transition, R_0 to T_{R_0}, remains ~ 2 μs. We conclude that our TR-WAXS data are not able to give definitive information on the time scale of the change in the CO rebinding rate from "fast" to "slow"; however, they unambiguously set the time scale of the main structural transition to ~ 2 μs.

parameter	value	error
$\tau_1 = 1/k_1$	2.1 μs	0.1 μs
$\tau_2 = 1/k_2$	20 μs	—
D_R	4.7 $\mu M^{-1} s^{-1}$	0.3 $\mu M^{-1} s^{-1}$
D_T	0.038 $\mu M^{-1} s^{-1}$	0.001 $\mu M^{-1} s^{-1}$
L_1	10	—
L_2	10^3	—
c_1	0.18	0.01
c_2	0.15	0.01
s_1	5	—
s_2	1.2	—

Table S2: Parameters obtained by the fitting procedure using the three state model, long dash in the error column indicates that the parameters has been kept fixed.
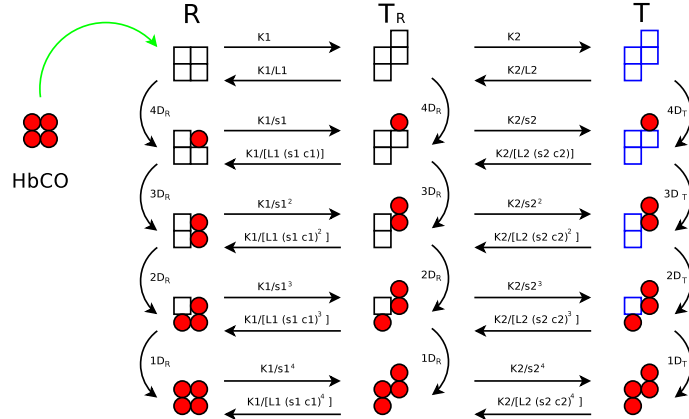

Figure S11: Scheme of the three-state kinetic model. Deoxy subunits are indicated as squares, CO-bound subunits as red circles. The border of the squares indicates the "fast-" (black) or "slow" (blue) recombining Hb subunits.
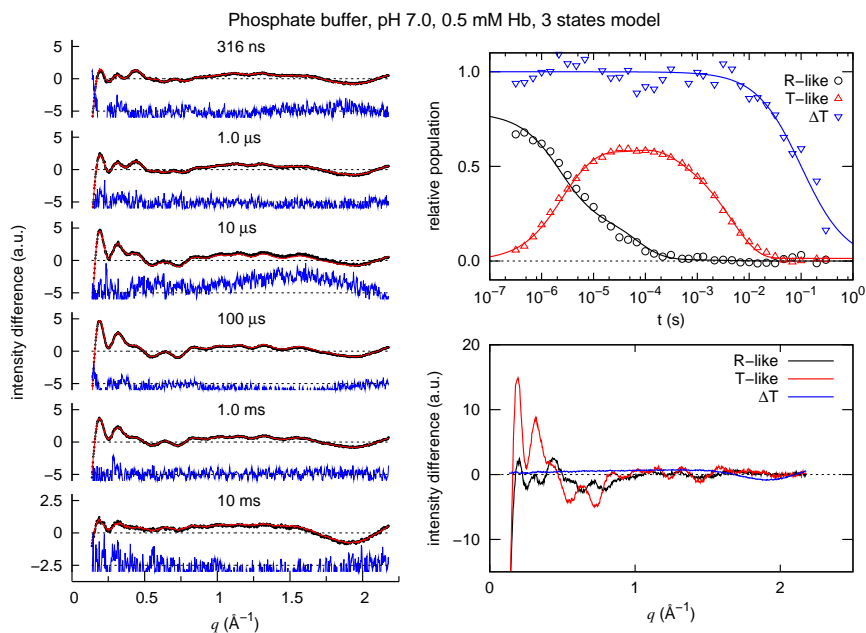
Figure S12: Fittings of data relative to the 0.5 mM Hb sample in 0.1 M phosphate buffer at pH 7 in terms of the three-state model. Right panels: (top) time dependence of R-like, T-like, and ΔT as calculated from the best fit parameters; (bottom) corresponding basis spectra.

S5. Assignment of the 147 ns signal to tertiary relaxations

S5.1. Time dependence

The intensity differences following photolysis by 2 ns laser have been collected for few time delays. Figure S13 shows them after subtraction of the heating signal; although some differences can be clearly seen (also thanks to the high S/N of the data) the curves are quite similar; assuming that the quaternary structure cannot have the time to change in few nanoseconds, these data suggest that the main origin of the signal at 147 ns is of tertiary origin.

S5.2. Dependence upon the percentage of deoxy hemes

A classical test to discriminate between tertiary and quaternary relaxations is their dependence upon the initial extent of photolysis; in fact, the amplitude of a tertiary event is expected to depend linearly on the percentage of deoxy hemes, while – before saturation – a more-than-linear dependence is expected for quaternary events, due to hemoglobin cooperativity. The data reported in Table 1 of the main text are of course indecisive in this respect, since variations in the parameter N_0 are too small to make meaningful comparisons. In view of its relevance, we made an "ad hoc" experiment to further investigate this point. To this purpose we repeated the experiment with 0.5 mM Hb in 0.1 M phosphate buffer pH 7, using the $\sim$2 ns pulses from a Nd:Yag laser to photolyze the sample. In the absence of multiple photolysis from a "long" laser pulse, a substantially lower percentage of deoxy hemes at $\sim$300 ns is expected, due to geminate rebinding. The results of this test experiment are reported in Figure S14. In panels a) and b) we report the difference signals at selected time delays measured with the "long" ($\sim$230 ns) and with the "short" ($\sim$2 ns) laser pulses, respectively. Note the different ordinate scales that evidence the different N_0 values in the two experiments; note also that in both panels the signal is fully developed already at 10 μs, indicating that the time scale of the quaternary transition is largely unaffected. In panel c) the signal measured at 300 ns with the 2 ns laser pulse (black curve) is multiplied by 1.33 and superimposed to the signal measured at the same time delay with the 230 ns laser pulse (red curve); the excellent agreement confirms the assignment of the difference signal to tertiary structural changes and indicates that about 60% of deoxy hemes is achieved (at 300 ns) with the 2 ns laser pulse. The same scaling factor was adopted for the data at 100 μs measured after photolysis by the 2 ns laser; this is reported in panel d) and clearly shows that the amplitude scales more than linearly with the extent of photolysis, in line with the cooperativity of the $R_0 \rightarrow T_0$ transition.
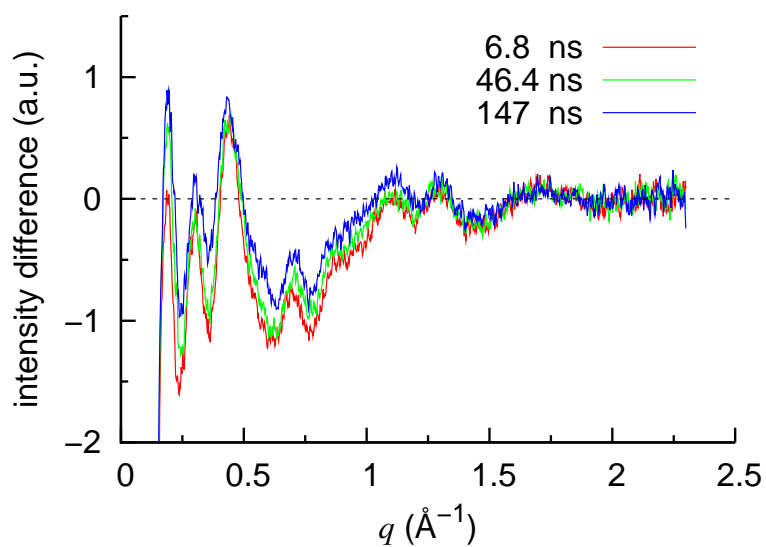
9

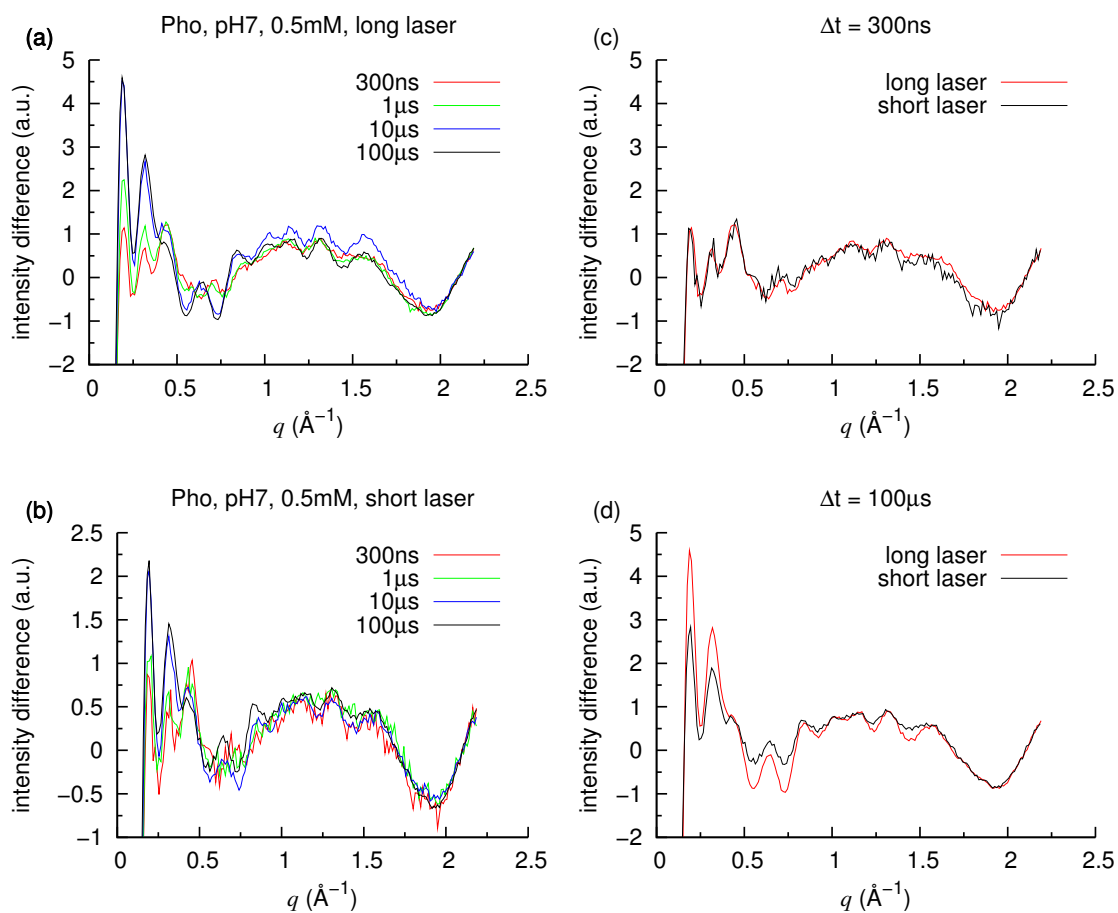Figure S13: Data obtained using a 2 ns photolysis laser

Figure S14: Comparison of data collected with 2 and 230 ns long laser photolysis pulse.

S6. Oxygen binding curves

Oxygen equilibrium curves of Hb in 0.1 M potassium phosphate at pH 7 were determined with standard spectrophotometric/tonometric methods at two different Hb concentrations, 25 μM and 0.5 mM (in tetramers), respectively. Other experimental condition were identical to those used for TR-WAXS measurements, except that a small amount (0.05% by weight) of Na-EDTA was added to reduce oxidation of the protein to the met-Hb form. A solution (4 ml) of oxyhemoglobin was introduced in a glass tonometer having the lower part sealed to a fused silica optical cuvette (cuvette light path = 1 cm, tonometer volume = 205 ml). The system was deoxygenated by alternatively exposing it either to vacuum or to pure nitrogen, while the tonometer (placed in a horizontal position) was slowly rotated inside a thermostated bath at 22 °C. Periods of 1.5 min were allowed between evacuation steps. Complete deoxygenation was checked spectrophotometrically with a Jasco V-570 spectrophotometer equipped with a Peltier thermostatted cell regulated so as to maintain the sample at 22 °C. Oxygenation of the sample was achieved by introducing in the tonometer known volumes of air at atmospheric pressure with a gas-tight syringe. After each addition, the solution was left to equilibrate with the gas phase for at least 10 min while slowly rotating the tonometer inside a water bath at 22 °C. After equilibration, the absorption spectrum of the sample was recorded in the desired wavelength range (470-670 nm or 600-830 nm depending on the Hb concentration used). Complete oxygenation of the sample was achieved by opening the tonometer and exposing the sample to air at atmospheric pressure. For samples at low (25 μM) Hb concentration, the percentage saturation (y) at a given oxygen partial pressure (pO_2) was calculated with the method of Benesch & Benesch [8], i.e. by averaging the results of the following two equations:

$$y = \frac{(OD_{540} - OD_{540}^{deoxy}) + (OD_{560} - OD_{560}^{deoxy})}{(OD_{540}^{oxy} - OD_{540}^{deoxy}) + (OD_{560}^{oxy} - OD_{560}^{deoxy})} \tag{4}$$

and

$$y = \frac{(OD_{576} - OD_{576}^{deoxy}) + (OD_{560} - OD_{560}^{deoxy})}{(OD_{576}^{oxy} - OD_{576}^{deoxy}) + (OD_{560}^{oxy} - OD_{560}^{deoxy})} \tag{5}$$

where OD_λ^{deoxy} and OD_λ^{oxy} are the optical densities of the sample (background subtracted optical absorption) at complete deoxygenation and complete oxygenation, respectively. For the experiments at high (0.5 mM) Hb concentration, the spectral region extending between 600 and 830 nm was used. The percentage saturation was calculated from the optical densities at 670 and 760 nm. by using equation 4. The oxygen partial pressure inside the tonometer was calculated from the amount of air introduced (V_{syr}), the partial pressure of oxygen in the air (p_{syr}), and the volume of the gas phase in the tonometer (V_{gas}). For samples at high Hb concentrations, a correction for the amount of oxygen bound to the protein was introduced. Including this correction term, one has that:

$$pO_2 = \frac{p_{syr}V_{syr}}{V_{gas}} - \frac{n_{heme}\, y\, R\, T}{V_{gas}} \tag{6}$$

where n_{heme} is the number of moles of hemes contained in the sample, and R and T are the gas constant and absolute temperature respectively. The amount of met-Hb contained in the sample was estimated spectrophotometrically (from the absorption at 630 nm) and was found to be always less than 5%.

References

[1] M. Cammarata, M. Levantino, F. Schotte, P. A. Anfinrud, F. Ewald, J. Choi, A. Cupane, M. Wulff, H. Ihee, Tracking the structural dynamics of proteins in solution using time-resolved wide-angle X-ray scattering, Nature Methods 5 (10) (2008) 881–886. `doi:10.1038/nmeth.1255`.

[2] M. Cammarata, L. Eybert, F. Ewald, W. Reichenbach, M. Wulff, P. Anfinrud, F. Schotte, A. Plech, Q. Kong, M. Lorenc, B. Lindenau, J. Raebiger, S. Polachowski, Chopper system for time resolved experiments with synchrotron radiation, Rev. Sci. Instrum. 80 (1) (2009) 015101. `doi:10.1063/1.3036983`.

[3] C. A. Sawicki, Q. H. Gibson, Quaternary conformational changes in human hemoglobin studied by laser photolysis of carboxyhemoglobin, J. Biol. Chem. 251 (6) (1976) 1533–1542.

[4] W. J. Fader, Density perturbations caused by weak absorption of a laser pulse, J. Appl. Phys. 47 (1976) 1975–1978. `doi:10.1063/1.322922`.

[5] J. W. Eaton, Octave, http://www.octave.org.

[6] R. B. Davies, C++ matrix manipulation library, http://www.robertnz.net/nm11.htm.

[7] CERN, Minuit minization library, http://lcgapp.cern.ch/project/cls/work-packages/mathlibs/minuit/index.html.

[8] R. Benesch, G. Macduff, R. E. Benesch, Determination of oxygen equilibria with a versatile new tonometer, Anal. Biochem. 11 (1) (1965) 81–87. `doi:10.1016/0003-2697(65)90045-X`.